Human and Passive Lower-Limb Exoskeleton Interaction Analysis: Computational Study with Dynamics Simulation using Nonlinear Model Predictive Control

Conference Paper · September 2023

DOI: 10.23919/SICE59929.2023.10354196

5 authors, including:

Naoto Haraguchi
Tokyo Metropolitan University
7 PUBLICATIONS **5** CITATIONS
SEE PROFILE

Ali Nasr
36 PUBLICATIONS **217** CITATIONS
SEE PROFILE

Keaton A. Inkol
University of Waterloo
15 PUBLICATIONS **98** CITATIONS
SEE PROFILE

Kazunori Hase
Tokyo Metropolitan University
279 PUBLICATIONS **983** CITATIONS
SEE PROFILE

Human and Passive Lower-Limb Exoskeleton Interaction Analysis: Computational Study with Dynamics Simulation using Nonlinear Model Predictive Control

Naoto Haraguchi[1†], Ali Nasr[2], Keaton A. Inkol[2], Kazunori Hase[1] and John McPhee[2]

[1]Department of Mechanical Systems Engineering, Tokyo Metropolitan University, Tokyo, Japan
(Tel: +81-42-677-1801; E-mail: haraguchi-naoto1@ed.tmu.ac.jp)
[2]Department of Systems Design Engineering, University of Waterloo, Ontario, Canada

Abstract: Forward dynamics simulations have the advantage of assessing performance of novel exoskeleton designs at a low cost. For developing a new passive lower-limb exoskeleton, the simulation needs to represent the sitting posture in which the wearer performs working tasks while maintaining balance with the whole body. The present study constructed a forward dynamics simulation for analyzing and developing a new passive lower-limb exoskeleton; the validity of the simulation was investigated using experimental data. The present method computes the interactions between the exoskeleton and wearer, such as reaction forces, physical posture, and physical load, based on the forward dynamics simulation driven by nonlinear model predictive control (NMPC). The NMPC cost function consisted of the physical load and the fitness of working task with constraints to evaluate balance. As a result, the present simulation represented the characteristic posture when sitting on the exoskeleton in which the wearer performs the working task while maintaining balance with the whole body. However, the simulation computed an upright posture of the lumbar joint that differed from the experimental results and needs to be improved. In future work, the simulation will be modified for representing the valid physical posture when wearing the exoskeleton, such as simulating the physical motion of the same working task as in the experiment, and modeling the interaction between the human, exoskeleton, and ground.

Keywords: Biomechanical analysis, Multibody model, Model-based design, Optimization, Balance control

1. INTRODUCTION

Passive lower-limb exoskeletons, as shown in Fig. 1, that reduce the physical load by supporting the body mass during standing work have been developed to prevent musculoskeletal disorders. The load on the lower limbs for workers who perform prolonged standing work can be reduced by performing work while sitting on one of these devices [1]. In contrast, a previous study reported that the risk of low back pain is higher due to the increase in lumbar load caused by leaning forward of the trunk when wearing the exoskeleton [2]. Therefore, a new passive lower-limb exoskeleton needs to be developed to reduce the lower limb load while preventing the increase in lumbar load by improving the forward learning posture.

The present study focuses on a design method for developing a new passive lower-limb exoskeleton. Forward dynamics simulations have the advantage in developing an exoskeleton as they can reasonably predict and be used to analyze the interaction between the human and the exoskeleton at a low cost without prototypes and experiments. However, in current simulations, the human model is driven by the experimental kinematic data, i.e., tracking optimization [3]. Therefore, the current simulations can lead to optimizing the exoskeleton structure for a given human posture but not the posture itself, making them unsuitable for developing passive lower-limb exoskeletons that improve lumbar loading when the user leans forward. Furthermore, considering the characteristic posture when sitting on the exoskeleton, the simulation needs to represent the sitting posture in which the wearer performs a working task while maintaining balance with the whole body. Therefore, a new forward dynamics simulation method, which can predict the characteristic posture in wearing the exoskeleton, is effective for developing a new passive lower-limb exoskeleton by optimizing the physical posture.

For application to developing a new passive lower-limb exoskeleton, the present study attempts to develop a new forward dynamics simulation that analyzes the interaction between the wearer and the exoskeleton by optimizing the physical posture. In this paper, we report on methods and validation of the results of the simulation driven by nonlinear model predictive control (NMPC) to determine the characteristic posture when wearing the exoskeleton.

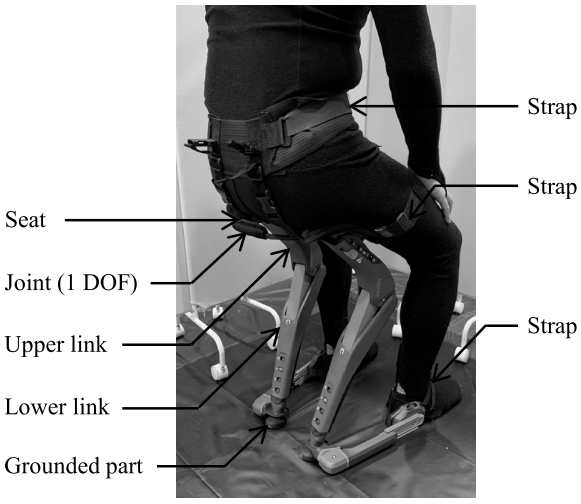

Fig. 1 Passive lower-limb exoskeleton (Chairless-Chair®; noonee AG, Switzerland). DOF: degree of freedom.

† Naoto Haraguchi is the presenter of this paper.

2. METHODS

The present method computes the interaction between the passive lower-limb exoskeleton and the wearer using a dynamics simulation that accepts the user body height and mass, working conditions, and the exoskeleton structure. Considering the issues of passive lower-limb exoskeletons, which include a lack of consideration for physical posture of the wearer, we constructed a simulation that computes the posture based on the NMPC without experimental kinematics data, as shown in Fig. 2. Moreover, for representing the goal of maintaining balance, the NMPC includes constraints to prevent the human-exoskeleton multibody model from falling; this model was developed in MapleSim 2022 (Maplesoft, Canada).

2.1 Human-exoskeleton model

We constructed the human-exoskeleton model combining a passive lower-limb exoskeleton model and a computational human model, which is shown in Fig. 3. There are a total of 15 rigid links for the whole human-exoskeleton system.

The human model consists of 13 segments such as the head, trunk, pelvis, upper arms, forearms-and-hands, thighs, shanks, and feet. The link length, the moment of inertia, and the center of mass of the human body were determined using a formula based on Japanese body height and mass [4, 5]. The body height and mass were defined as 1.75 m and 65.0 kg, respectively, which was the average for the participants during the experiment performed to verify the validity of the simulation. We used the exoskeleton model shown in Fig. 1 digitized by a 3D scanner (ATOS Core 200; GOM GmbH, Germany).

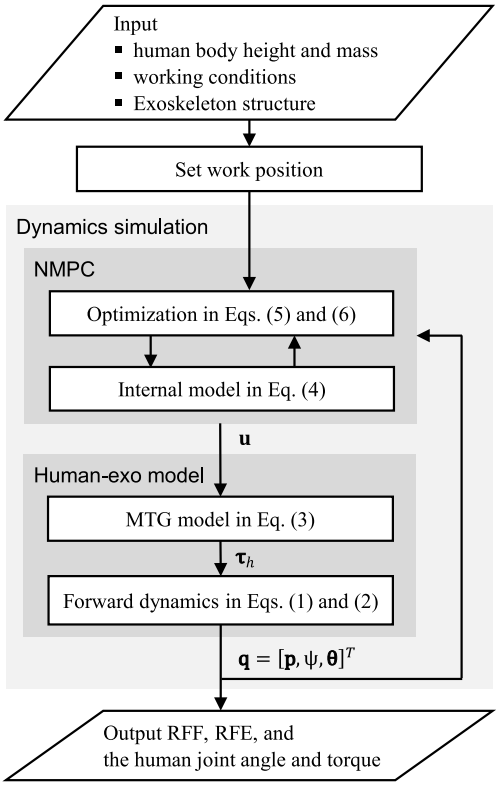

Fig. 2 Simulation process. The simulation consists of nonlinear model predictive control (NMPC) and human-exoskeleton (exo) model including muscle torque generator (MTG) and forward dynamics calculation. The simulation outputs the reaction forces acting on the foot (RFF) and the exoskeleton (RFE) and the joint angle and torque.

The exoskeleton was modeled separately for the left and right legs and connected to the rear surface of each thigh. The connection between the thigh and the exoskeleton was modeled as one rotational degree of freedom (DOF) in sagittal plane. The position of the connection point was placed 60 mm from the hip joint on the thigh, which was determined by referring to the exoskeleton structure shown in Fig. 1. The relative angle between the upper link and lower link was set to 90º, which was the same as the angle during the experiment performed to verify the validity of the simulation. In the present study, although the exoskeleton shown in Fig. 1 has straps that are worn around the waist and thigh, the straps were not modeled because these straps connect the human to the exoskeleton when not sitting on the device, i.e., standing or moving. In addition, the foot and the grounded part of the exoskeleton were constrained by a strap and link with variable lengths from 100 to 260 mm so that the foot and the grounded part of the exoskeleton would not be separated by more than the maximum length of the link. In this study, we modeled the positional relationship between the foot and the grounded part of the exoskeleton by constraining the grounded part to the ground 260 mm behind the foot.

The overall model has 17 coordinates, $\mathbf{q}=[\mathbf{p}, \psi, \boldsymbol{\theta}]^T \in \mathbb{R}^{17}$, which represents the generalized coordinate vector consisting of the joint angles and the three DOFs between the pelvis and the global coordinates. The neck, lumbar, shoulder, elbow, hip, knee, and ankle joints have one DOF for flexion-extension and dorsiflexion-plantarflexion and the joint between the exoskeleton and the thigh segment has one DOF for flexion-extension ($\boldsymbol{\theta} \in \mathbb{R}^{14}$).

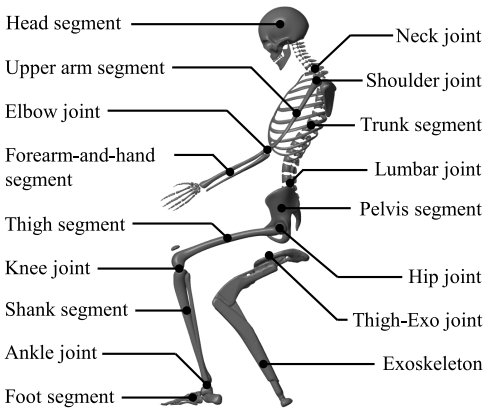

Fig. 3 Human-exoskeleton model. All human joints have one rotational degree of freedom (DOF) and the joint between the thigh and the exoskeleton (Thigh-Exo joint) has one rotational DOF in sagittal plane. Relative to an inertial frame, the pelvis has three DOFs, which are vertical and anterior translational DOFs and sagittal rotational DOF.

The pelvis has three DOFs between the global coordinates, which are vertical and anterior translational DOFs and sagittal rotational DOF $[\mathbf{p}, \psi]^T \in \mathbb{R}^3$.

The equation for the forward dynamics simulation is represented by the generalized coordinate vector $\mathbf{q}$ as follows:

$$\mathbf{M}\ddot{\mathbf{q}} + \mathbf{\Gamma}(\mathbf{q}, \dot{\mathbf{q}}) + \mathbf{\Phi}_q{}^T\boldsymbol{\lambda} = \boldsymbol{\tau}, \quad (1)$$

$$\mathbf{\Phi}(\mathbf{q}) = \mathbf{0}, \quad (2)$$

where $\mathbf{M} \in \mathbb{R}^{17\times17}$ is the mass matrix and $\mathbf{\Gamma} \in \mathbb{R}^{17}$ is a vector consisting of Coriolis, centrifugal, and gravitational effects. $\mathbf{\Phi} \in \mathbb{R}^{10}$ consists of 10 position-level kinematic constraint equations, where 6 equations represent the vertical and anterior translational constraints and the sagittal rotational constraint on each foot and ground, and 4 equations represent the vertical and anterior translational constraints on each exoskeleton and ground. The Jacobian matrix $\mathbf{\Phi}_q = \partial\mathbf{\Phi}/\partial\mathbf{q} \in \mathbb{R}^{10\times17}$ maps the Lagrange multipliers vector $\boldsymbol{\lambda} \in \mathbb{R}^{10}$, which represents the reaction forces and moments, to constraint forces and moments as dictated by each element of $\mathbf{q}$. The generalized coordinate vector $\mathbf{q}$ and the Lagrange multipliers vector $\boldsymbol{\lambda}$ were calculated by the joint torque vector $\boldsymbol{\tau} \in \mathbb{R}^{17}$ based on Eqs. (1) and (2). These equations were provided as differential-algebraic equations (DAEs) due to the closed kinematics chains. The model was constructed using MATLAB/Simulink (MathWorks, Inc., USA) and used the *ode45* variable-step solver.

After computing the state variable vector $\mathbf{q}$, the forward kinematics calculates the position and posture of each segment. Subsequently, the hand distance d_h and the gaze distance d_g are obtained to evaluate the fitness of the human posture to labor work, which is shown in Fig. 4. d_h represents the distance between the work position and the distal point of the lower arm segment, and d_g is defined as the vertical coordinate of the work position in the eye coordinate placed at the head segment. The position of the eye coordinate was determined by the relative positions of the head and eye [6]. The eye coordinate was set to be at a 10º inclination to the head coordinate [7]. The work position was fixed at a height of 765 mm from the ground and a distance of 413 mm from the center of mass of the pelvis segment, which were the average values obtained in the experiment performed to verify the validity of the simulation.

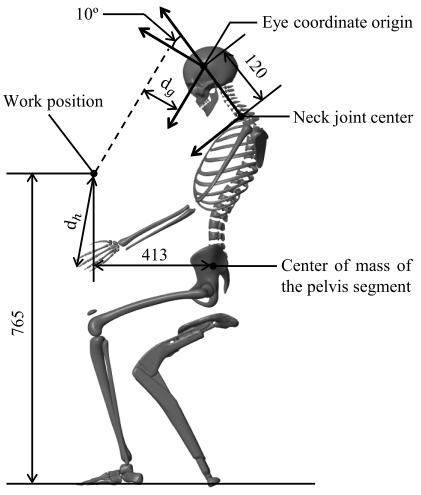

Fig. 4 Definitions of the hand desitance d_h and the gaze distance d_g. Units: mm.

2.2 Muscle torque generator model

The torque at a *j*th joint τ^j, which is a component of $\boldsymbol{\tau}$, is offered by a muscle torque generator (MTG) model that imitates the performance of all muscles around a given joint without the need for modeling individual muscle geometries and forces [8-10]. The MTG model consists of an active component (generates the active torque limited by the joint angle and angular velocity) and a passive component (representing the joint's viscosity and range of motion), as follows:

$$\tau^j = \mathrm{u}_+^j\tau_{0,+}^j\tau_{\theta,+}^j(\mathbf{q})\tau_{\omega,+}^j(\dot{\mathbf{q}}) + \mathrm{u}_-^j\tau_{0,-}^j\tau_{\theta,-}^j(\mathbf{q})\tau_{\omega,-}^j(\dot{\mathbf{q}}) + \tau_p^j(\mathbf{q}, \dot{\mathbf{q}}), \quad (3)$$

where τ_p^j is the passive torque represented by the damping term and the double exponential function to increase the limiting torque near the anatomical joint limits, which were defined by related research [11-14]. τ_0^j is the peak isokinetic torque, which was obtained by related anthropometric measures [15-19]. τ_θ^j is the angle-scaling function represented in the literature using a second-order polynomial function or trigonometric function [8, 19]. τ_θ^j is normalized by the maximal isometric torque of each joint, i.e., the value of the τ_θ^j at the optimum angle is 1. τ_ω^j is the angular velocity-scaling function represented in the literature using some parameters [8, 19]. τ_ω^j is also normalized by the maximal isometric torque of each joint, i.e., the value of τ_ω^j is 1 at 0 rad/s velocity. τ_0^j, τ_θ^j, and τ_ω^j were defined separately for the positive and negative directions. $\tau_{\theta,+}^j$, $\tau_{\theta,-}^j$, $\tau_{\omega,+}^j$, and $\tau_{\omega,-}^j$ have positive values, $\tau_{0,+}^j$ has a positive value, and $\tau_{0,-}^j$ has a negative value. Moreover, the joint torque τ^j is amplified by the activation signals $\mathrm{u}_+^j(t) \in [0,1]$ and $\mathrm{u}_-^j(t) \in [0,1]$ determined by the NMPC, which is described in Section 2.3.

2.3 Nonlinear model predictive control

The present method aims to simulate the characteristic posture when wearing the passive lower-limb exoskeleton, in which the wearer performs a working task while maintaining balance with the whole body. Thus, the present simulation needs to control the human movements for multiple tasks through multiple joint motions. Basically, these complex human movements are coordinated by the central nervous system with a complex signal that is computed with two sections of motion prediction and corrective command [20]. The NMPC has the advantage of controlling the human movements in wearing the exoskeleton because it has functions of the feedforward and feedback controls, which is similar to the function of the central nervous system, and can control a multi-input multi-output system [21].

The NMPC employs an internal model from the human model to simulate human-exoskeleton dynamics,

which is computed by the state vector $\mathbf{x} = [\mathbf{q}, \dot{\mathbf{q}}]^T \in \mathbb{R}^{34}$ and control input vector $\mathbf{u} = [u_+^1, \cdots, u_+^{17}, u_-^1, \cdots, u_-^{17}]^T \in \mathbb{R}^{34}$, as follows:

$$\dot{\mathbf{x}} = \mathbf{F}(\mathbf{x}(t), \mathbf{u}(t), t), \tag{4}$$

where $\mathbf{F} \in \mathbb{R}^{34}$ is the nonlinear system function representing the human-exoskeleton dynamics based on Eqs. (1–3). The internal model is used to simulate the human-exoskeleton dynamics within the prediction horizon $[t_0, t_f]$ and determine the input $\mathbf{u}(t_0)$ that minimizes the cost function J under constraints, as follows:

$$J = \int_{t_0}^{t_f} \left\{ w_1 {d_h}^2 + w_2 {d_g}^2 + w_3 \sum_{j=1}^{17} \left({u_+^j}^2 + {u_-^j}^2 \right) + w_4 \sum_{j=1}^{17} \left({\dot{u}_+^j}^2 + {\dot{u}_-^j}^2 \right) \right\} dt, \tag{5}$$

$$\mathbf{h}(\mathbf{x}(t), \mathbf{u}(t)) \leq \mathbf{0}, \tag{6}$$

where w_1, w_2, w_3, and w_4 are weight factors, which were set to $w_1 = 1$, $w_2 = 1$, $w_3 = 0.01$, and $w_4 = 0.01$, respectively, as determined empirically. The prediction horizon was set to 0.3 seconds and contained 3 nodes as determined empirically. The cost function J contributes to generating a biomechanical valid posture for labor tasks. In addition, Eq. (6) represents the stability constraints to prevent the zero moment point (ZMP) from moving outside the base of support (BOS) boundaries formed by the foot and exoskeleton, slipping of the feet and grounded part of the exoskeletons (assuming a static coefficient of friction of 1.0), the vertical ground-reaction forces from pulling on the feet and grounded part of the exoskeletons, and the center of pressure of each foot from moving outside the BOS boundaries formed by the foot.

After computation, the reaction force acting on the feet (RFF), the reaction force acting on the exoskeletons (RFE), and the human joint angle and torque were computed by the simulation. The vertical forces of the RFF and RFE were calculated based on the reaction force $\boldsymbol{\lambda}$, which were normalized by the body mass of the human model and the gravitational acceleration, i.e., the percentage body mass. The joint angle and torque in the sagittal plane at the lumbar, hip, knee, ankle, and neck were calculated based on $\boldsymbol{\theta}$ and $\boldsymbol{\tau}$. In the present study, the simulation time was set to 20 seconds, which is a sufficient time for the system to reach a stationary solution, and the states for the system at 20 seconds were output as results.

2.4 Experiment

To verify the validity of the simulation, we experimented using the passive lower-limb exoskeleton. The participants were 12 healthy males (height: 1.75±0.06 m, mass: 65.0±8.0 kg, age: 24.3±3.1 years). The study was approved by the Ethics Committee of Tokyo Metropolitan University. The participants remained in a relaxed posture while wearing the exoskeleton and performed an experimental task, which was to assemble two plates with bolts and nuts using a ratchet wrench. The working time was set to 80 s. The work height and work distance were set according to the physique and posture of each participant [22]. The motion capture system (OptiTrack Flex3; Natural Point Inc., USA) measured the three-dimensional coordinates of markers attached to the whole body. Data were digitally filtered (low-pass filter, fourth-order, -3 dB at 6 Hz, Butterworth) and were sampled at 100 Hz. The force acting on the foot was measured by a mobile force plate system (M3D-FP-U; Tec Gihan Co., Ltd., Japan). The force acting on the thigh from the seat of the exoskeleton was measured by a six-axis force sensor (USX10-H10-500N; Tec Gihan Co., Ltd., Japan) [2]. Data were digitally filtered (low-pass filter, fourth-order, -3 dB at 18 Hz, Butterworth) and sampled at 1,000 Hz.

We analyzed the RFF, RFE, joint angle, and joint torque. We calculated the vertical forces of the RFF and RFE by measurement data for the mobile force plate system and the six-axis force sensor, which were normalized by the body mass and gravitational acceleration, i.e., percentage body mass, of each participant. In addition, we analyzed the joint angle in the sagittal plane at the lumbar, neck, hip, knee, and ankle dominant joints. The lumbar joint angle was determined by the line passing through the L5 marker and the T10 marker, and the line passing through the C7 marker and the T3 marker. The neck joint angle was determined by the line passing through the C7 marker and the T3 marker, and the line passing through the C7 marker and the tragus marker. The joint angles at the hip, knee, and ankle were analyzed by inverse kinematics using standard, open-source musculoskeletal model analysis software, OpenSim 4.1 [23]. We used a previously developed musculoskeletal full-body model [24]. Moreover, we analyzed the joint torque in the sagittal plane at the lumbar, neck, hip, knee, and ankle dominant joints. The joint angles at the lumbar spine (L4L5), hip, knee, and ankle were analyzed by inverse dynamics using OpenSim 4.1 [23, 24]. The neck joint torque was calculated as the product of the moment arm between the center of the neck joint and the center of the head mass and the head weight. The center of the neck joint was defined as the midpoint between the marker at C7 and the clavicle [25]. The center of the head mass was estimated to be 17% of the distance from the mid-tragus (midpoint of the left and right tragus markers) to the top of the head marker [26]. The head mass was calculated by an estimation based on the head circumference and body mass [27]. All data were averaged for all measurement times.

3. RESULTS

The RFF, RFE, joint angles, and joint torques obtained by the experiment and the simulation are shown in Fig. 5. The simulation results for the joint angles and torques at the knee and ankle were within the range of the average and standard deviation of the experimental results. In contrast, the simulation results for the RFF, the RFE, and the joint angles and torques at the lumbar, neck, and hip were outside the range of the average and standard deviation of the experimental results. In addition, the physical posture of a participant during the experiment and the model posture generated by the simulation are shown in Fig. 6. The simulation computed a physical posture in which the wearer sits on the exoskeleton while the hands and gaze are directed to the work position.

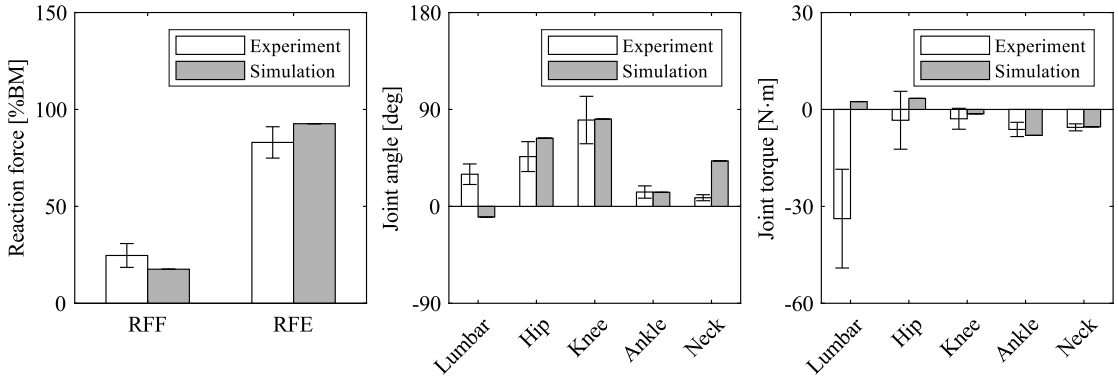

Fig. 5 (left) Vertical reaction force acting on foot (RFF) and exoskeleton (RFE). Values are normalized by body mass and gravitational acceleration, i.e., percentage body mass (%BM). (middle) Joint angles. The flexion and dorsiflexion angles are positive. (right) Joint torques. The flexion and dorsiflexion torques are positive. The results of the experiment are the average and standard deviation for all participants.

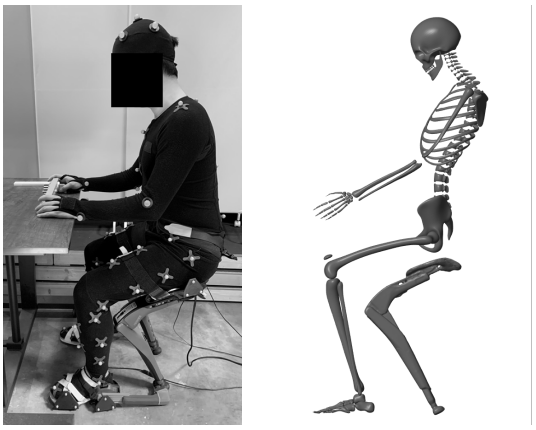

Fig. 6 (left) Physical posture of the participant during the experiment. (right) Model posture generated by the simulation.

4. DISCUSSION

The simulation represented the sitting posture when wearing the passive lower-limb exoskeleton in which the wearer directs the hand and gaze toward the work position while maintaining balance to prevent falling. The present method using the NMPC contributed to simulating this characteristic posture in wearing the exoskeleton; the posture was computed by the NMPC which consists of the cost function including the error between the work position and the hand and gaze and the constraint including an evaluation of balance using the ZMP. Thus, the present method using the NMPC has the advantage of simulating the characteristic posture when wearing the passive lower-limb exoskeleton. In addition, the present simulation computed the physical posture based on the input of the working condition (the work position for directing the hand and gaze), not experimental kinematic data. Therefore, the present method has the potential to compute the optimal posture when wearing a new passive lower-limb exoskeleton without depending on the experimental kinematic data and is effective for developing the new exoskeleton that requires improvement of the wearer's posture to prevent increasing physical loads.

Although the present method is expected to be applied to analyzing and developing a new passive lower-limb exoskeleton, the simulation currently needs to be improved because the simulation results have some differences from the experimental results. For instance, a nearly upright posture with a small lumbar torque was observed in the simulation because the NMPC computed a physical posture that minimized the cost function including the muscular activations of the whole body. In contrast, it has previously been reported that the participants wearing the exoskeleton took a forward-leaning posture, which increased lower limb and lumbar loads compared to an upright posture, to prevent falling backward, although they were instructed to take a relaxed posture [1, 2]. Moreover, a previous study has reported that an increase in the lumbar joint compression force due to higher lumbar joint torque when wearing the exoskeleton leads to an increase in the risk of low back pain [2]. Therefore, the present simulation needs to accurately predict the lumbar joint torque in order to develop a new passive lower-limb exoskeleton based on analyzing this kinetic factor, and the simulation's accuracy needs to be improved by computing a valid posture of the wearer when wearing the exoskeleton.

In future work, we plan to modify the simulation and the model to represent conditions similar to those of wearing the exoskeleton. First, the work position, which was set as the fixed value in this study, will be variable with time to simulate the movement of the COG of the whole body caused by movements with the working task. This change might represent a situation in which the COG of the whole body easily moves outside the BOS boundaries formed by the foot and exoskeleton and contribute to generating a physical posture that is close to that of the experimental results. Second, although the human and exoskeleton were modeled as only multibody dynamics in this study, a new model that consists of the multibody dynamics model and contact model will be constructed in future work. Modeling collisions between the human, exoskeleton, and ground might represent situations in which the wearer needs to take a stable posture to prevent falling and is effective for generating a valid posture when wearing the exoskeleton.

5. CONCLUSION

We developed a new forward dynamics simulation method for analyzing the interactions between a passive lower-limb exoskeleton and the wearer by optimizing physical posture using an NMPC. The present method simulated the characteristic posture in wearing the exoskeleton with an NMPC, which includes the cost function evaluating working task and physical load and the constraints evaluating the balance of the wearer. The present simulation, which can compute the posture of the wearer without experimental kinematic data, has the potential to be used for developing a new passive lower-limb exoskeleton that requires improvement of the wearer's posture. However, the simulation currently needs to be improved because the simulation results have minor differences from the experimental results. In future work, we plan to modify the simulation and the model to improve the validity of the present method, such as representing actual walking tasks and modeling collisions between the human, exoskeleton, and ground.

REFERENCES

[1] T. Luger et al., "Influence of a passive lower-limb exoskeleton during simulated industrial work tasks on physical load, upper body posture, postural control and discomfort", *Appl. Ergon.*, Vol. 80, pp. 152–160, 2019.

[2] N. Haraguchi and K. Hase, "Biomechanical analysis based on a full-body musculoskeletal model for evaluating the effect of a passive lower-limb assistive device on lumbar load", *J. Biomech. Sci. Eng.*, Vol. 18, No. 3, 23-00024, 2023.

[3] M. Harant et al., "Cost function evaluation for optimizing design and actuation of an active exoskeleton to ergonomically assist lifting motions", *2019 IEEE-RAS 19th International Conference on Humanoid Robots*, pp. 186–193, 2019.

[4] M. Ae et al., "Estimation of inertia properties of the body segments in Japanese athletes", *SOBIM Japan* (in Japanese), Vol. 11, pp. 23–33, 1992.

[5] R. Drillis et al., "Body segment parameter: A survey of measurement techniques", *Artif. Limbs*, Vol. 8, No. 1, pp. 329–351, 1964.

[6] M. Kouchi and M. Mochimaru, "Anthropometric database of Japanese head 2001", National Institute of Advanced Industrial Science and Technology, H16PRO-212, 2008.

[7] F. E. Mount et al., "Evaluation of neutral body posture on shuttle mission STS-57 (SPACEHAB-1)", NASA TM-2003-104805, 2003.

[8] A. Nasr et al., "Scalable musculoskeletal model for dynamic simulations of upper body movement", *Comput Methods Biomech Biomed Engin*, 2023.

[9] K. A. Inkol et al., "Muscle torque generators in multibody dynamic simulations of optimal sports performance", *Multibody Syst. Dyn.*, Vol. 50, pp. 435–452, 2020.

[10] M. Millard et al., "A reduced muscle model and planar musculoskeletal model fit for the simulation of whole-body movements", *J. Biomech*, Vol. 89, pp. 11–20, 2019.

[11] D. T. Davy and M. L. Audu, "A dynamic optimization technique for predicting muscle forces in the swing phase of gait", *J. Biomech*, Vol. 20, No. 2, pp. 187–201, 1987.

[12] A. E. Engin, "On the biomechanics of the shoulder complex", *J. Biomech*, Vol. 13, No. 7, pp. 575–581, 1980.

[13] A. E. Engin and S. M. Chen, "Kinematics and passive resistive properties of human elbow complex", *J. Biomech. Eng.*, Vol. 109, No. 4, pp. 318–323, 1987.

[14] M. H. Pope et al., "Experimental measurements of vertebral motion under load", *Orthop. Clin. North Am.*, Vol. 8, No. 1, pp. 155–167, 1977.

[15] S. Kumar, "Isolated planar trunk strengths measurement in normals: Part III — Results and database", *Int. J. Ind. Ergon.*, Vol. 17, No. 2, pp. 103–111, 1996.

[16] A. N. Vasavada et al., "Three-dimensional isometric strength of neck muscles in humans", *Spine*, Vol. 26, No. 17, pp. 1904–1909, 2001.

[17] R. E. Hughes et al., "Age-related changes in normal isometric shoulder strength", *Am J Sports Med*, Vol. 27, No. 5, pp. 651–657, 1999.

[18] L. A. Frey-Law et al., "Knee and elbow 3D strength surfaces: Peak torque-angle-velocity relationships", *J. Appl. Biomech.*, Vol. 28, No. 6, pp. 726–737, 2012.

[19] D. E. Anderson et al., "Maximum voluntary joint as a function of joint angle and angular velocity: Model development and application to the lower limb", *J. Biomech.*, Vol. 40, pp. 3105–3113, 2007.

[20] N. Mehrabi et al., "Predictive simulation of reaching moving targets using nonlinear model predictive control", *Front. Comput. Neurosci.*, Vol. 10, 143, 2017.

[21] A. Nasr et al., "Model-based mid-level regulation for assist-as-needed hierarchical control of wearable robots: a computational study of human-robot adaptation", *Robotics*, Vol. 11, No. 1, 20, 2022.

[22] T. Luger et al., "Subjective evaluation of a passive lower-limb industrial exoskeleton used during simulated assembly", *IISE Trans. Occup. Ergon. Hum. Factors*, Vol. 7, No. 3–4, pp. 175–184, 2019.

[23] S. L. Delp et al., OpenSim: Open-source software to create and analyze dynamic simulations of movement", *IEEE Trans. Biomed. Eng.*, Vol. 54, No. 11, pp. 1940–1950, 2007.

[24] M. E. Raabe and A. M. W. Chaudhari, An investigation of jogging biomechanics using the full-body lumbar spine model: Model development and validation, *J. Biomech*, Vol. 49, No. 7, pp. 1238–1243, 2016.

[25] K. R. Syamala et al., Armrests and back support reduced biomechanical loading in the neck and upper extremities during mobile phone use, *Appl. Ergon.*, Vol. 73, pp. 48–54, 2018.

[26] A. N. Vasavada et al., Gravitational demand on the neck musculature during tablet computer use, *Ergonomics*, Vol. 58, No. 6, pp. 990–1004, 2015.

[27] C. E. Clauser et al., Weight, volume, and center of mass of segments of the human body, *Wright-Patterson Air force Base*, AMRL-TR-69-70, 1969.